Industrial Crops & Products 237 (2025) 122138

Contents lists available at ScienceDirect

Industrial Crops & Products

journal homepage: www.elsevier.com/locate/indcrop

Low-dosage foliar application of nanosized macro- and micro- nutrients for enhanced yield of high-quality Rosemary oil

Chalasani Danteswari [a,b,1], Pullabhotla V.S.R.N. Sarma [a,1], Harita Pant [b], Mahadevakumar Shivannegowda [c], Dharani Kumar Chennamsetty [b], Venkata Sreenivasulu Kummari [b], Vijaya Ranganath Chenna [d], Siddaiah Chandra Nayaka [e], Shaikshavali Petnikota [f,*], Challapalli Subrahmanyam [g], Venkata Satya Siva Srikanth Vadali [b,*], Appa Rao Podile [a,*]

[a] School of Life Sciences, University of Hyderabad, Hyderabad 500046, India
[b] School of Engineering Sciences and Technology, University of Hyderabad, Hyderabad 500046, India
[c] Botanical Survey of India (BSI), Andaman Nicobar Regional Centre, Port Blair 744102, India
[d] Charles Renard Analytical Laboratory, International Crops Research Institute for the Semi-Arid Tropics (ICRISAT), Hyderabad 502324, India
[e] Department of Studies in Biotechnology, University of Mysore, Mysuru 570006, India
[f] Biomass Technology Centre, Department of Forest Biomaterials and Technology, Swedish, University of Agricultural Sciences, Umeå SE-90183, Sweden
[g] Department of Chemistry, Indian Institute of Technology Hyderabad, Sangareddy 502285, India

ARTICLE INFO

Keywords:
Nutrients
Fertilizers
Nanoscale
Foliar spray
Rosemary
Essential oil

ABSTRACT

The quantum of nutrients supplied for efficient Rosemary plant growth and high-quality essential oil (EO) yield is relatively high, posing an environmental hazard. Therefore, developing nutrient management strategies that reduce environmental impact while maintaining or enhancing Rosemary plant growth, bio-fortification, secondary metabolite content, and EO yield is imperative. In this line, this work reports a simple mechanical milling strategy that enables low-dosage foliar application of nanosized macro-nutrient and micro-nutrient particles for extraordinary Rosemary plant growth, bio-fortification, enhanced secondary metabolites, and high-quality EO yield even at a considerably lower nutrient supply. Even for a much lower dosage than the recommended dosage, a considerable increase in the total plant weight and in nitrogen (N), iron (Fe), manganese (Mn), zinc (Zn), and copper (Cu) content in plant shoots, in excellent correlation with their enhanced availability on the surface of the nanosized nutrient particles, is achieved. More importantly, an increase in the concentration of 1,8-cineole (a key metabolite in EO and the quality descriptor of EO) in EO extracted from the plants cultivated using nanoscaled nutrients at much lower inputs is achieved. The enhanced concentration of 1,8-cineole is attributed to the increased presence of Zn, Mn, and Cu, which elicit specific pathways for synthesizing 1,8-cineole in plants. This work offers a simple, scalable, sustainable alternative strategy to conventional high-nutrient-input agricultural practices.

1. Introduction

Rosemary (*Rosmarinus officinalis* L.) is a fragrant evergreen Lamiaceae shrub renowned worldwide for its phytotherapeutic attributes (Afshar et al., 2022; Ali et al., 2020; Ribeiro-Santos et al., 2015). Although native to the Mediterranean region (Heinrich et al., 2006; Ulbricht et al., 2010), it is also cultivated in non-native regions primarily to meet the exiguous domestic consumption (Hammer and Junghanns, 2020; Rathore et al., 2022). Of late, Rosemary's cultivation in non-native regions has gained popularity due to a substantial increase in demand from the food, cosmetic, and pharmaceutical industries. Consequently, farmers in these regions want to expand the cultivation of Rosemary and find methods to increase its yield. Prudent nutrient management during their cultivation is one viable method for the success (i.e., adaptation, expansion, and maturation) of Rosemary-like crops in non-native lands (Shan et al., 2022). This method of

* Corresponding authors.
E-mail addresses: shaikshavali.petnikota@slu.se (S. Petnikota), vvsssse@uohyd.ac.in (V.S.S.S. Vadali), podilerao@uohyd.ac.in (A.R. Podile).
[1] Equal contribution

https://doi.org/10.1016/j.indcrop.2025.122138
Received 13 April 2025; Received in revised form 10 October 2025; Accepted 15 October 2025
Available online 22 October 2025

supplying vital nutrients results in enhanced soil fertility, augments crop productivity and quality, preserves nutrient equilibrium, and bolsters resistance to local environmental stress, pests, and diseases (Chen et al., 2023; Weinmann et al., 2023). Typically, the common macro-nutrients, namely, Nitrogen (N), Phosphorus (P), and Potassium (K) are provided for leaf growth and overall plant health; root development, flowering, and fruiting; and water intake and nutrient absorption, respectively (Chen et al., 2023; Grusak and DellaPenna, 1999; Shan et al., 2022; Weinmann et al., 2023). Similarly, the micro-nutrients, namely, zinc (Zn), iron (Fe), copper (Cu), manganese (Mn), boron (B), and molybdenum (Mo), are provided to improve the overall health of the plants and avoid any physiological disorders (Chen et al., 2023; Grusak and DellaPenna, 1999; Shan et al., 2022; Weinmann et al., 2023). In cultivating the Rosemary crop in non-native lands, locally recommended dosages of macro- and micro-nutrients are applied to improve the herbage and oil yield (Ayoob et al., 2023; Mehrabani et al., 2018; Mwithiga et al., 2022; Puttanna et al., 2010). By applying NPK (a popular commercial fertilizer and the source of macro-nutrients) (Ayoob et al., 2023; Mwithiga et al., 2022; Puttanna et al., 2010), and Zn (one of the micro-nutrients) (Mehrabani et al., 2018), the Rosemary crop yield significantly improved in terms of its essential oil (EO) yield and metabolite content in the extracted oil. However, although very effective, NPK must be applied in huge quantities (100–300 kg/ha annually) to cultivate Rosemary (Ayoob et al., 2023; Mwithiga et al., 2022; Puttanna et al., 2010). On the other hand, micro-nutrients do not need to be applied in the same quantity as NPK, but applying these even in a slight excess can be toxic to the soil where the plants are cultivated (Grusak and DellaPenna, 1999). In this context, nano-fertilizers emerged to improve crops' yields by improving crops' nutrition and nutrient use efficiency (NUE) even with substantially low fertilizer input (Bekah et al., 2025; Ding et al., 2023; Jakhar et al., 2022; Lowry et al., 2024; Mim et al., 2025; Pudhuvai et al., 2025). If made small enough, the nano-fertilizer particles can directly infiltrate the outer layers of plant cells, facilitating a significantly enhanced effectiveness in nutrient uptake and NUE (Guo et al., 2018).

Therefore, nano-NPK preparation and its foliar application to enhance Rosemary crop yield, if any, were undertaken in this work. Additionally, the non-availability (only that of Zn is available) (Mehrabani et al., 2018) of literature on using micro-nutrients in the cultivation of the Rosemary crop prompted us also to take up the preparation of nanosized particles of micro-nutrient mixture (MNM) and their systematic testing in combination with nanosized particles of NPK to enhance the Rosemary crop yield in terms of its EO yield and metabolite content in the extracted oil, if any. A simple mechanical milling method was used to prepare nano-NPK and nano-MNM particles. It may be noted that the higher the content of 1,8-cineole, a predominant metabolite in the Rosemary EO, the greater the oil quality (in both native (Dhouibi et al., 2023) and non-native (Laiq-ur-Rahman et al., 2007) cases). The subsequent objective was to see if applying nanosized nutrients increases the proportion of 1,8-cineole in the extracted Rosemary EO. This work's experimental observations and corresponding analyses demonstrated that applying nanosized NPK and MNM particles led to extraordinary Rosemary plant growth, biofortification, and a high-quality Rosemary EO yield at substantially low nutrient input. The analyses also established the correlation between the enhanced yield and the standard plant growth descriptors (and nutrients' supply and their use). This work lays the groundwork for developing easy strategies to apply nanosized nutrients, thereby maximizing plant growth and yield while minimizing fertilizer usage.

2. Materials and methods

2.1. Preparation of nanosized NPK and MNM particles

The commercial fertilizers, 19:19:19 NPK, and micro-nutrient mix (Utkarsh Combi-2) were procured from IFFCO (India) and Utkarsh Agrochem Pvt. Ltd. (India). These fertilizers were independently milled using a high-energy shaker mill (8000D Mixer/Mill, SPEX SamplePrep LLC, USA). In each case, a balls-to-fertilizer ratio of 5:1 by weight was considered. Before milling the samples, the stainless steel (SS) milling jars were thoroughly cleaned following the standard operating procedures. Dry milling was carried out using SS balls for 45 min. The milled fertilizers were characterized to check for size reduction and changes in surface composition (compared with the as-procured fertilizers) and were used for Rosemary plant growth experiments.

2.2. Characterization of samples

JEOL JEM-F200 transmission electron microscope (TEM), operated at an accelerating voltage of 200 kV, was used to record the feature sizes of the as-processed samples to assess the quantum of size reduction due to milling. Fourier transform infrared (FTIR) spectroscopy was performed to check for surface compositional changes in the as-processed samples. IR transmission and absorbance data were collected and analyzed according to the standard procedure for all samples (Baudot et al., 2010; Jayawardena et al., 2021). To assess any changes in composition due to size reduction, the attenuated total reflectance (ATR)-FTIR transmission spectra of all the samples were recorded using the iD7 Thermo Scientific Nicolet 5 spectrometer, while the absorbance spectra were recorded using the PerkinElmer Frontier spectrometer. The FTIR spectra were collected in fingerprint and diagnostic wavenumber ranges. The X-ray photoelectron spectroscopy (XPS) data of all the samples were recorded and analyzed to understand the bonding structure on the surfaces of as-processed fertilizer particles compared with the as-procured fertilizers (Moulder et al., 1992). The XPS data were recorded using Thermo-Fisher Scientific's K-Alpha XPS system with a resolution of ~0.5 eV. Surface charge compensated data was analyzed by peak-fitting using the Gaussian or Voigt profiles, depending on the original spectral profile. Only the best-fit data was considered for analysis. XPS data were analyzed to quantify the nutrients on the surfaces of Nano-NPK and Nano-MNM particles compared with NPK and MNM particles. The colloidal stability of the Nano-NPK and Nano-MNM suspensions was determined by analyzing the respective zeta potential data. The suspensions were prepared by dispersing Nano-NPK and Nano-MNM particles in DI water. Zeta potential measurements were carried out using Anton Paar's Litesizer 500 analyzer.

2.3. Plant growth experiments and analysis

One-month-old Rosemary saplings, maintained in a suitable greenhouse without any fertilizer supply, were considered for plant growth experiments. Standard pot experiments were conducted with three saplings per pot. Foliar application of the fertilizers (i.e., spraying the fertilizers directly on the leaves) was used. Different dosages of fertilizers were provided to the plants: i) recommended dosage (RD) - the application of a blend of NPK (i.e., the macro-nutrients) and the MNM (i.e., the micro-nutrients) of 250 ppm each (positive control), which the local farmers use to cultivate the Rosemary crop, and ii) new dosage (ND) – the application of a blend of mechanically milled NPK and the MNM of 0.25, 2.5, 25, 50, 75, 100, and 125 ppm each corresponding to a dosage of 0.1, 1, 10, 20, 30, 40, and 50 % of RD. All dosages were administered every four weeks for three months under greenhouse conditions. The fertilizers were sprayed in the early morning hours until the leaves of the plants were drenched. Rosemary plants were also grown by providing only water (i.e., without any fertilizers) under greenhouse conditions. The plant growth experiments were conducted with 3 replicates for each dosage. Standard practices were followed to harvest the plants and quantify their growth and development characteristics, including shoot and root lengths, total fresh and dry weights, and nutrient availability in the plants. Before estimating the nutrient availability in the plants, the harvested plants were thoroughly cleaned with water and dried in a hot air oven at 40°C for 2 h. The well-cleaned

random shoot samples were used to estimate the nutrient availability. The availability of four nutritional elements, Fe, Zn, Ca, and Mg, was estimated by nitric acid and hydrogen peroxide digestion accompanied by inductively coupled plasma optical emission spectrometry (ICP-OES, Teledyne Leeman Labs, HD Prodigy) (Wheal et al., 2011). The sulfuric acid-selenium digestion method was used to estimate the total nitrogen using the SKALAR SAN+ + SYSTEM Continuous Flow Analyzer (Sahrawat et al., 2002). The acquired data were subjected to the one-way analysis of variance (ANOVA) (Table Supplementary Material (SM)1), followed by Duncan's Multiple Range Test (DMRT), to measure differences between pairs of least-squares (LS) means (Mosa et al., 2021). A least significant difference of 0.05 % was selected and measured using Lumivero's XLSTAT to compare the different LS means.

2.4. Rosemary oil extraction and analysis

The EO samples were extracted from shade-dried leaves using Clevenger's apparatus through steam distillation, and the oil yield was monitored in different cases. Then, the metabolites in the EO samples were analyzed using the Agilent 8860 GC system equipped with a 58 cm× 54 cm x 49 cm column. The injector and detector temperatures were set to 250°C, with N_2 as the carrier gas. The injection volume was 1 µL. The retention time was estimated and determined using the standards (Merck, Germany).

3. Results and discussion

The TEM images (Fig. 1) of the milled commercial NPK (Figs. 1(a) and 1(b)) and MNM (Figs. 1(c) and 1(d)) samples showed nanoscale features, implying that the particle size decreased. It may be noted that the average particle size of the as-procured fertilizers (i.e., both NPK and MNM) is ~2 µm. In the case of the milled NPK, the finest features that could be resolved were 2–5 nm in size (Fig. 1(b)). However, these features consisted of larger nanoparticles, ~100–200 nm in size (Fig. 1(a)). In the case of the milled MNM, the finest features that could be resolved were ~20–50 nm in size (Figs. 1(c) and 1(d)). Therefore, the milled samples were correspondingly named Nano-NPK and Nano-MNM. The size reduction mechanism of NPK and MNM particles was similar to that of other inorganic materials. It involves various physical processes such as impact, shear, compression, and attrition (Pohshna et al., 2020; Suryanarayana, 2001). However, due to their mechanically soft nature, the milling time and energy input (in terms of milling speed, size of milling balls, milling media, type of milling, etc.) (Pohshna et al., 2020; Suryanarayana, 2001) as indicated by suitable modelling outcomes were considerably low to achieve an optimal size reduction. In the present case, the optimal time required to achieve the nanosized particles was less than one hour (while other milling parameters are modest), correlating well with the expected outcomes for soft materials.

The NPK sample considered in this work consisted of water-soluble 19 % N (~4 % nitrate nitrogen, ~4.5 % ammoniacal nitrogen, and ~10.5 % urea nitrogen), 19 % P_2O_5, and 19 % K_2O by weight as the source of macro-nutrients, which plants take up as NH_4^+/NO_3^-, $H_2PO_4^-/HPO_4^{2-}$ and K^+ ions when NPK is foliar sprayed (Chen et al., 2023; Grusak et al., 1999; Shan et al., 2022; Weinmann et al., 2023). The MNM sample considered in this work was composed of Ethylenediaminetetraacetic acid (EDTA) as the chelating agent and ~4 % Zn, ~2 % Fe, ~0.5 % Mn, ~0.54 % B, ~0.3 % Cu, and ~0.1 % Mo by weight as the micro-nutrients. However, the constituent water-soluble salts in the commercial MNM sample were undisclosed. Nonetheless, it is well-known that Zn, Fe, Cu, Mn, B, and Mo are taken up by plants as Zn^{2+}, Fe^{2+} or Fe^{3+}, Cu^{2+}, Mn^{2+}, $B(OH)_4^-$ and $H_2BO_3^-$, and MoO_4^{-2} ions when MNM is foliar sprayed (Chen et al., 2023; Grusak and DellaPenna, 1999; Shan et al., 2022; Weinmann et al., 2023). The ATR-FTIR spectra of Nano-NPK particles were compared with NPK particles in Fig. 2. The bands in the region 1300–1500 cm^{-1} (shown in Fig. 2(a)) correspond to the IR absorption due to different deformation and stretching modes in NH_4^+ and NO_3^-, while the one at ~828 cm^{-1} corresponds to the

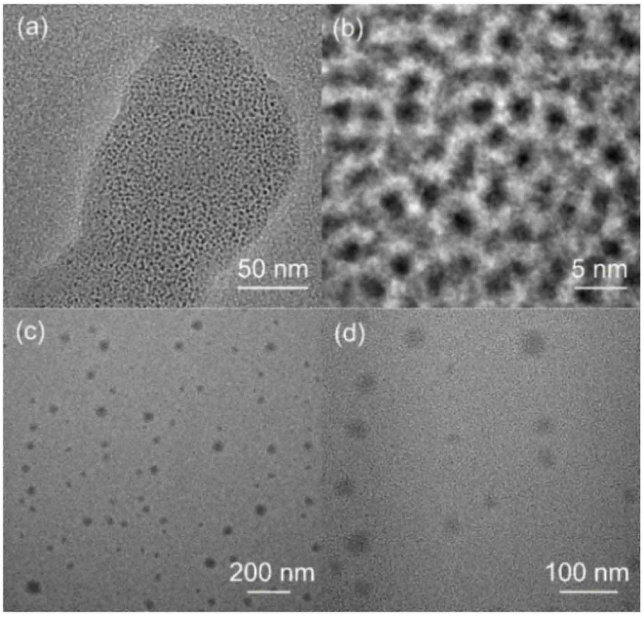

Fig. 1. TEM images of (a-b) Nano-NPK and (c-d) Nano-MNM particles.

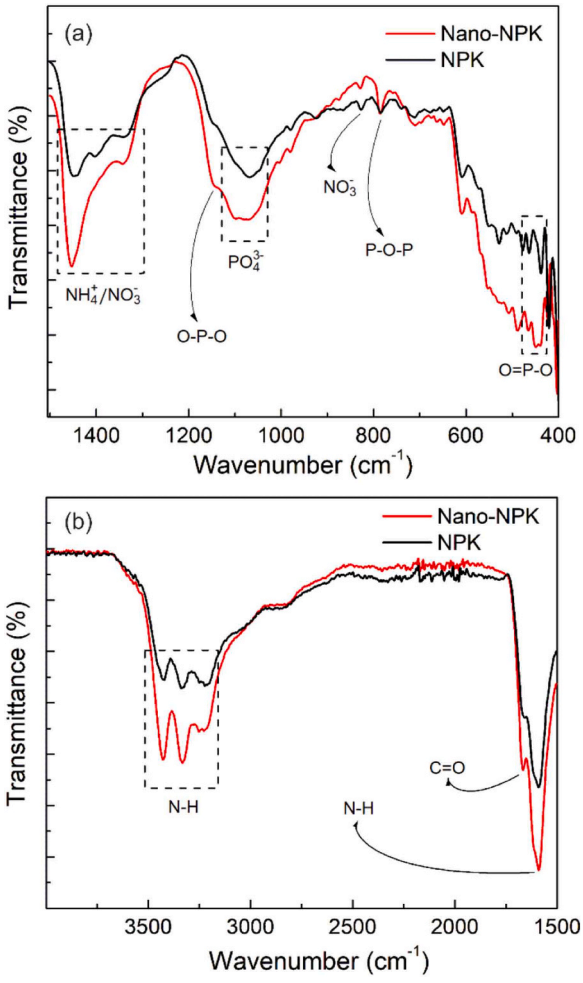

Fig. 2. ATR-FTIR spectra of NPK and Nano-NPK in (a) fingerprint and (b) diagnostic regions.

absorption due to the symmetric stretching mode in NO_3^- (Wu et al., 2007). The bands at ~1147, ~1080, and ~785 cm^{-1} and in the region ~440–469 cm^{-1} correspond to the IR absorption due to symmetric stretching modes of O −P −O in PO_2 units, symmetric stretching mode of PO_4^{3-} tetrahedra, symmetric stretching mode of P − O − P, and bending mode of O = P − O, respectively (Chahine et al., 2004; Magdas et al., 2008; Salim et al., 1995; Shih et al., 1999). The bands at ~3426, ~3333, and ~1590 cm^{-1} correspond to IR absorption due to stretching vibrations of N −H in urea (Timón et al., 2021), as shown in Fig. 2(b). The IR band at ~1667 cm^{-1} corresponds to absorption due to C═O stretching vibration in urea (Timón et al., 2021), as shown in Fig. 2(b). The ATR-FTIR spectra of Nano-MNM particles were compared with those of MNM particles shown in Fig. 3. The IR absorption bands (Fig. 3(a)) at ~438, ~466, ~534, and ~641 cm^{-1} correspond to Zn −O (Xiong et al., 2006), Cu −O (Kayani et al., 2015), Fe −O (Namduri and Nasrazadani, 2008), and Mn −O vibrations (Yang et al., 2005). The band at ~466 cm^{-1} also corresponds to Mn −O (Buciuman et al., 1999). The band at ~847 cm^{-1} corresponds to Mo = O (Nazri and Julien, 1992), and the one at ~1324 cm^{-1} corresponds to B −O stretching (Bellamy et al., 1958). The bands at ~927, ~1324, ~1395 (Fig. 3(a)), and ~1585 cm^{-1} (Fig. 3(b)) correspond to absorption due to C −C axial deformation, NH^+angular deformation, C −O vibrations, and asymmetrical axial deformation of COO^- in EDTA (Magdalena et al., 2018).

FTIR spectral analysis revealed that the bonding structures in the Nano-NPK and Nano-MNM particles were intact, implying that size reduction did not result in detrimental compositional changes. Additionally, the increased IR absorbance (Figs. SM1 and SM2) in the case of Nano-NPK and Nano-MNM samples compared with their bulk counterparts confirmed the increased number of surface bonds, a typical consequence of size reduction (Baudot et al., 2010; Jayawardena et al., 2021).

Further, in the X-ray photoelectron survey spectra (Fig. 4(a)) of NPK and Nano-NPK particles, N, P, K, and O peaks were observed (Moulder et al., 1992), and in the case of MNM and Nano-MNM particles, Zn, Fe, Cu, Mn, B, Mo, N, and O peaks (Fig. 4(b)) were observed (Moulder et al., 1992), consistent with the original nutrient composition and FTIR analysis. A careful analysis of the high-resolution scans of individual nutrients revealed interesting changes in the surface contents (especially those representative of macro- and micro-nutrients) of Nano-NPK and Nano-MNM particles. It may be noted that the unindexed X-ray photoelectron spectral peaks in Fig. 4(a) and (b) correspond to the elements in the carrier/chelating and undisclosed substances in the original samples. The quantitative analysis of XPS data of Nano-NPK and Nano-MNM (compared with their respective counterparts) showed subtle changes in the spectral features of certain elements, implying surface reconstruction (i.e., variations in the local electronic structure around the atoms on the surface and sub-surface (within a depth of a few to 10 nm)) in Nano-NPK and Nano-MNM samples, a consequence of size reduction (Baer and Engelhard, 2010; Fairley et al., 2021). On first look, it was

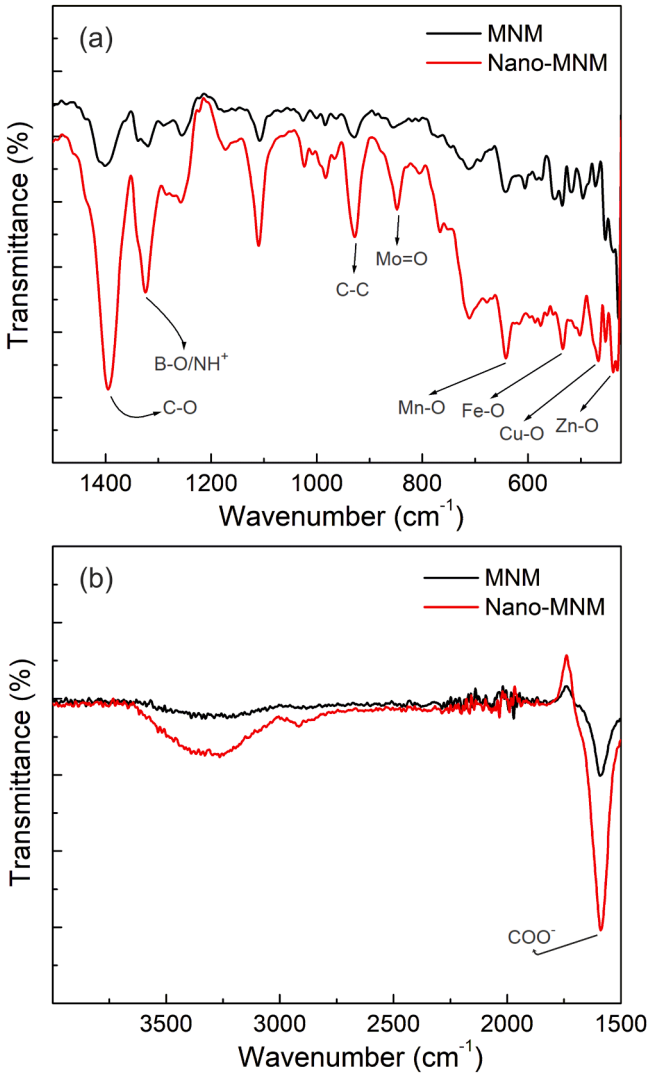

Fig. 3. ATR-FTIR spectra of MNM and Nano-MNM in (a) fingerprint and (b) diagnostic regions.

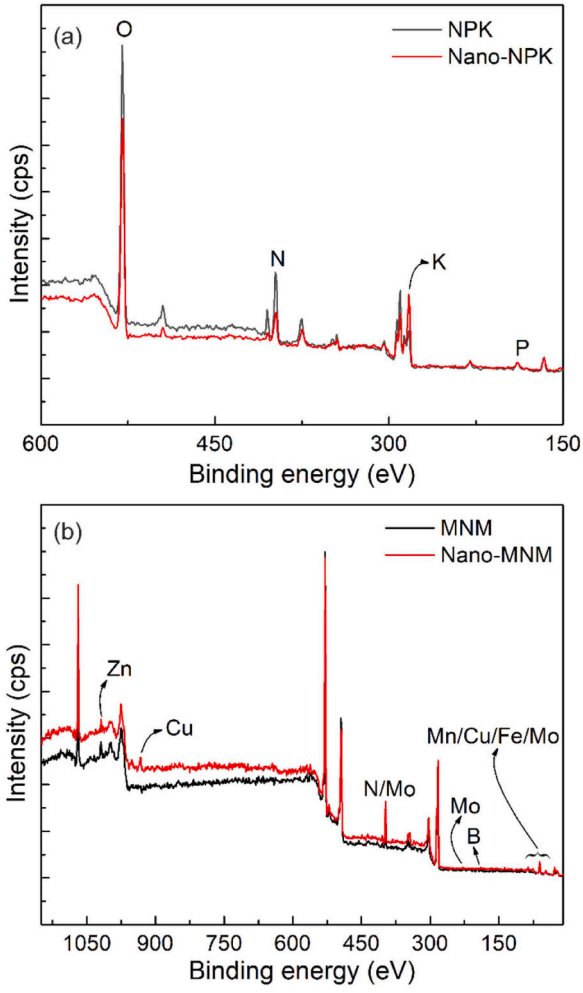

Fig. 4. X-ray photoelectron survey spectra of (a) NPK and Nano-NPK and (b) MNM and Nano-MNM samples.

observed that the intensities of most spectral signals from the main elements (i.e., the nutrients) decreased, contrary to the generally anticipated increase in intensities in nano-counterparts. This was attributed to increased adventitious atoms (here, C, O, and other unindexed atoms in the carrier/chelating substances) on the surface and sub-surface regions of Nano-NPK and Nano-MNM particles (Baer and Engelhard, 2010; Fairley et al., 2021). This scenario helps enhance the efficiency of carrier/chelating substances.

The quantitative analysis (Fig. SM3) in the binding energy (BE) range of 396–408 eV (corresponding to N 1 s X-ray photoelectron signal) revealed that the Peak Area by Integrating Dat% (Area IntgP) values were ~60.4 %, ~21.5 %, and ~18 % for N (Urea), N (Ammoniacal) and N (Nitrate) in the case of the NPK sample, while they were ~38.5 %, ~39 %, and ~22.5 %, respectively, in the case of the Nano-NPK sample, implying increased presence of ammoniacal and nitrate N on the surfaces of Nano-NPK particles compared with that of NPK particles, which in turn implying enhanced availability of ammoniacal and nitrate N for the plants to uptake. Since plant leaves uptake N in the NH_4^+ and NO_3^- forms, their enhanced availability on the surfaces of Nano-NPK particles facilitated supplying more N at less fertilizer input. It may also be noted that the order of efficient and quick uptake by the plant leaves is N (Nitrate) > N (Ammoniacal). Therefore, enhanced availability of N (Nitrate) and N (Ammoniacal) may also improve the NUE at less fertilizer input. However, supplying more than sufficient N (Ammoniacal) through foliar spraying can harm plant growth (Britto and Kronzucker, 2002; Esteban et al., 2016; Liu and von Wirén, 2017; Shilpha et al., 2023). However, no such detrimental observations were made regarding plant physiology or growth characteristics. In fact, if NH_4^+ toxicity is mitigated, N (Ammoniacal) should be the preferred form of N supply to plants because it is more energy- and metabolically- efficient than N (Nitrate) because its intrinsic form is ready for use in amino acid metabolism (Jackson et al., 2008; Mokhele et al., 2012). The quantitative XPS analyses in the BE ranges of 127–134 eV (corresponding to P 2p X-ray photoelectron signal from P_2O_5) (Fig. SM4) and 288–296 eV (corresponding to K 2p X-ray photoelectron signal from K_2O) (Fig. SM5) revealed slightly decreased peak intensities in the case of Nano-NPK compared with NPK, implying that the slightly reduced availability of P and K on the surfaces of Nano-NPK particles, as reflected in the available P and K values measured in harvested Rosemary plant shoots. The N 1S (Fig. SM3), P 2p (Fig. SM4), and K 2p (Fig. SM5) X-ray photoelectron signals in the case of Nano-NPK were slightly shifted to the lower BE side compared with NPK, indicating that the surface chemical environment of the former (as indicated by FTIR analysis) has changed (Baer and Engelhard, 2010; Fairley et al., 2021).

The quantitative analysis (Fig. SM6) in the BE range of 1015–1050 eV (corresponding to Zn 2p X-ray photoelectron signal) revealed that the Area IntgP values were ~66.16 % and ~33.84 % for $2p_{3/2}$ and $2p_{1/2}$ in the case of the MNM sample, while they were ~41.6 % and ~58.37 %, respectively, in the case of the Nano-MNM sample, implying the increased presence of Zn (in the higher oxidation state, i.e., in the form of Zn^{2+} containing compound) on the surface of Nano-MNM particles because Area IntgP value is directly proportional to the number of atoms contributing to $2p_{1/2}$ peak. Also, Zn^{2+} exhibits a higher BE for the $2p_{1/2}$ peak, as shown in Fig. SM6. More importantly, enhanced availability of Zn in the Zn^{2+} state is most desirable for the plants to efficiently uptake Zn when Nano-MNM is foliar-sprayed. An interesting revelation in this work is the substantial increase in the availability of Cu (in +2 oxidation state) on the surface of Nano-MNM particles. In the case of MNM particles, Cu was not discernible even though 0.3 % by weight is present in them, implying poor Cu surface availability. Figure SM7 shows the detection of Cu $2p_{1/2}$ and Cu $2p_{3/2}$ signals in the case of Nano-MNM and their absence in the case of MNM. The high-resolution scan in the BE region of 227–235 eV revealed that the typical Mo 3d ($3d_{3/2}$ and $3d_{5/2}$) signals could not be resolved in both the MNM and Nano-MNM cases, likely because Mo is present at only 0.1 % by weight, which was probably below the detection limitation. The Mo 3d peak might be present but greatly broadened due to the local chemical environment on the surfaces of MNM and Nano-MNM particles, making it difficult to distinguish. Even though Mo is indicated in Fig. 4(b), the confidence level is poor because the instrument did not resolve Mo 3d XPS signals, while Mo 3p XPS signals in the BE range 395–401 eV had a strong interference with N 1 s signals (corresponding to the presence of EDTA). However, the Mo $3p_{3/2}$ XPS signal could be resolved using peak-fitting (Fig. SM8), indicating its presence (in the +6 oxidation state) on the surface of MNM and Nano-MNM particles. The quantitative analysis (Fig. SM9) in the BE range of 40–55 eV (corresponding to Mn 3p and Fe 3p X-ray photoelectron signals) revealed that the Area IntgP values were ~86.36 % and ~13.64 % for Mn 3p and Fe 3p in the case of the MNM sample, while they were ~85.32 % and ~14.68 %, respectively, in the case of the Nano-MNM sample, implying the slightly increased presence of Fe on the surface of Nano-MNM particles. Figure SM10 shows the detection of B 1 s signals in the BE range 184–196 eV in both MNM and Nano-MNM samples. However, in the Nano-MNM sample, the B 1 s signal corresponding to B (Bromide) could not be resolved using peak-fitting, implying that the B (Boric acid) content significantly increased on the surface of Nano-MNM particles. This observation w.r.t B showed enhanced availability of suitable B form for plants to uptake it. The change in the surface presence of Zn, Cu, Fe, Mn, and B in Nano-MNM is reflected in their availability in harvested Rosemary plant shoots.

Figures SM11 and SM12 show the O 1 s XPS signals in both NPK and nano-NPK and MNM and Nano-MNM samples, respectively. Figure SM11 shows reduced O 1 s peak intensity in the case of Nano-NPK compared with NPK, while Figure SM12 shows that the O 1 s peak intensity was almost the same in the case of MNM and Nano-MNM, implying that unintended surface oxidation was not encountered during dry milling of the NPK and MNM. Also, as discussed, except for the increase in intensity of the XPS signals corresponding to the elements N, P, and K (in the case of Nano-NPK compared with NPK), and Zn, Mn, and B (in the case of Nano-MNM compared with MNM), no other elements showed increase in their signal intensity, implying increase in surface availability of N, P, K, Zn, Mn, and B (without unintended oxidation).

Figures SM13 and SM14 show the relative frequency (%) versus zeta potential values (in V) of Nano-NPK and Nano-MNM suspensions. The mean zeta potential values of Nano-NPK and Nano-MNM suspensions are −39.97 mV and −32.24 mV, respectively, indicating that the suspensions can be classified as stable long-term nanosuspensions (Kamble et al., 2022; Serrano-Lotina et al., 2023).

The photographs of the Rosemary plants grown by applying different dosages of macro- and micro-nutrients (indicated as ND) of the Nano-

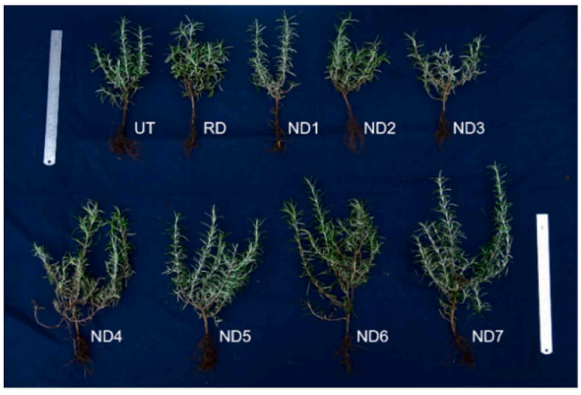

Fig. 5. Photographs of the representative Rosemary plants grown by foliar spraying different dosages of nutrients and harvested after 12 weeks. ND1, ND2, ND3, ND4, ND5, ND6, and ND7 correspond to 0.1, 1, 10, 20, 30, 40, and 50 % of RD. RD is the application of the blend of NPK and the MNM of 250 mg/L each (positive control). UT represents untreated.

NPK and Nano-MNM and RD are shown in Fig. 5, which also shows the untreated (UT) case, wherein only water was supplied. All the plants shown in Fig. 5 were harvested after 12 weeks.

Applying specific dosages (ND4-ND7) of Nano-NPK and Nano-MNM resulted in visually enhanced herbage (i.e., plant biomass) (Fig. 6). To quantify the same, the plant growth characteristics, namely, shoot and root lengths and fresh and dry plant weights in each case, were measured and shown in Fig. 6. It can be observed from Fig. 6(a) that ND5, ND6, and ND7 resulted in an almost 1.5-fold increase in shoot length compared with the RD case, and even ND3 and ND4 resulted in ~1.15–1.3-fold increase in shoot length compared with the RD case. A similar trend in the increase of root length (Fig. 6(b)), fresh weight (Fig. 6(c)), and dry weight (Fig. 6(d)) was observed. From these observations, it can be inferred that compared with RD, ND of only 20 % of the RD was sufficient for enhanced plant growth and development, and ND5 (only 30 % of the RD) was optimal among all the dosages when all plant growth characteristics are considered simultaneously.

It may be noted that even ND1 (0.1 % of RD) and ND2 (1 % of RD) resulted in better plant growth and development than the UT case, indicating that there were no compositional changes due to size reduction and, therefore, the nanosized fertilizer particles are still effective in plant growth and development. The observations presented in Figs. 5 and 6 about the enhanced Rosemary plant growth and development indicate improved NUE due to the application of the nanosized NPK and MNM particles, as hypothesized in the introduction. To confirm and quantify the improved NUE, shade-dried shoots of the harvested Rosemary plants (shown in Fig. 5) were analyzed for macro- and micro-nutrient availability. Table 1 shows the quantities of different macro- and micro-nutrients available in the shoots of the Rosemary plants. From Table 1, it was clear that the nutrient availability (both macro and micro) increased in the case of RD compared with the UT case, correlating well with enhanced plant growth characteristics due to the increase in NUE as a consequence of the application of RD of macro- and micro-nutrients. More importantly, Table 1 showed that N (macro-nutrient) and Fe, Zn, and Cu (micro-nutrients) content increased in the cases of ND5, ND6, and ND7, indicating enhanced NUE by the plants even at lower dosages than the RD. This observation also correlates well with the enhanced surface availability of N, Fe, Zn, and Cu in the respective nanosized nutrient particles, as revealed by X-ray photoelectron spectral analysis. For better clarity, N, Fe, and Zn content in the shoots of the harvested Rosemary plants as a function of different dosages used to grow the Rosemary plants are shown in Fig. 7, which clearly shows that the highest average values were observed in the case of ND7 (50 % of the RD). However, a closer observation of Table 1 and Fig. 7 indicated that ND5 (only 30 % of the RD and 20 % less than ND7) was optimal among all the dosages when all the nutrients are considered simultaneously.

Further, to assess the yield and quality of the Rosemary oil as a result of the application of different dosages of Nano-NPK and Nano-MNM compared with the RD of their bulk counterparts, the EO was extracted from shade-dried leaves of all the different plants, and the total oil yield and metabolite content in each case were analyzed. Fig. 8 shows the Rosemary oil yield (in μL per 100 g of dried leaves) from different Rosemary plants. It shows that the Rosemary oil yield is higher in the RD case than in the UT case, reiterating the use of supplying macro- and micro-nutrients to the plants and, more so, if the dosage can be lower than RD (Ayoob et al., 2023; Mehrabani et al., 2018; Mwithiga et al., 2022; Puttanna et al., 2010). In this regard, it can be observed from Fig. 8 that the Rosemary oil yield has increased in the ND3 to ND7 cases compared with RD.

Enhanced oil yield was attributed to the increased herbage, resulting from enhanced nutrient supplementation through typical fertilizer input to Rosemary plants (Ayoob et al., 2023; Puttanna et al., 2010). Here, the enhanced nutrient supplementation (as revealed by plant shoot-composition analyses) and higher oil yield were achieved by applying nanosized nutrients at much lower dosages, reiterating the expediency of nano-fertilizers (Guo et al., 2018; Jakhar et al., 2022). Additionally, the foliar application of nutrients (also used here) to medicinal, aromatic, and other commercial crops gives an added advantage (Ahmed et al., 2023a; Ahmed et al., 2023b; Cao et al., 2022; Elmer et al., 2021; Ghodrati-Tazangi et al., 2023; Hao et al., 2021; Hassanpour-aghdam et al., 2020; Li et al., 2023; Mehrabani et al., 2018; Rostami et al., 2021; Reshma and Meenal, 2022; Sharma et al., 2022; Tawfeeq et al., 2016; Xu et al., 2023). The foliar application effectively supplies nutrients to plants through their leaves, primarily when a quick amendment of nutrient deficiencies is needed or when soil conditions are suboptimal. However, care must be taken regarding the supply of RD to ensure optimal NUE, avoiding the risk of leaf burn or other adverse

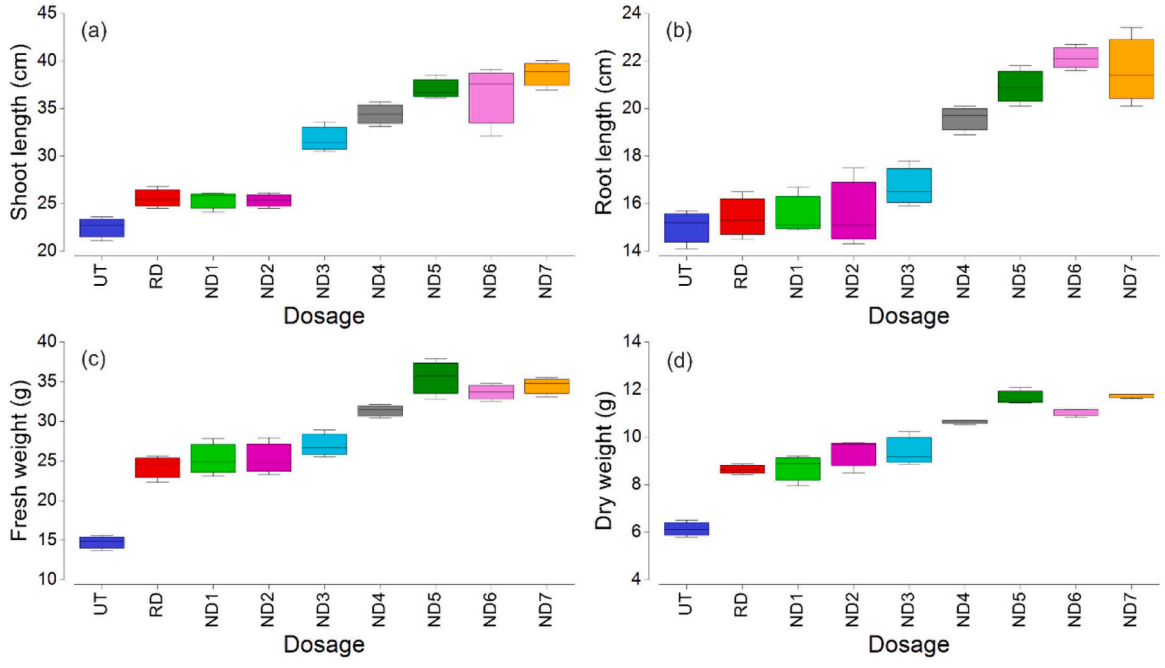

Fig. 6. Plant growth characteristics ((a) Shoot length, (b) Root length, (c) Fresh weight, and (d) Dry weight) of the Rosemary plants (shown in Fig. 5).

Table 1
Macro- and micro-nutrient contents in the shoots of the Rosemary plants (shown in Fig. 5). A summary of the LS mean values calculated by ANOVA followed by DMRT using XLSTAT, USA, is shown. The significance of the LS mean values is also shown.

Dosage	N Quantity (ppm)	P	K	Fe	Zn	B	Cu	Mn
ND1	12472.135°	1113.743°	15631.621°	2035.202°	41.213°	22.671°	60.518°	72.927°
ND2	13398.998**	1263.094**	14946.098**	2247.841**	38.830**	31.762**	84.646**	69.036**
ND3	12859.986***	1244.956***	14785.198***	2297.306***	38.914***	29.440***	76.457***	88.000***
ND4	12196.836**	1188.185**	15725.475**	3647.526**	39.111**	30.574**	84.580**	85.333**
ND5	14644.643***	1317.836***	15746.302***	3638.403***	44.134***	30.073***	102.562***	107.667***
ND6	14148.873***	1395.627***	15650.790***	3844.273***	42.330***	30.635***	96.322***	111.333***
ND7	14817.901***	1401.201***	17179.652***	3936.995***	55.359***	37.227***	106.499***	116.000***
RD	13343.029***	1338.710***	17703.308***	2604.550***	43.912***	30.081***	76.736***	152.667***
UT	12882.866°	1066.435°	15231.604°	2335.722°	34.555°	27.447°	49.956°	63.909°
Pr > F (Model)	< 0.0001***	< 0.0001***	< 0.0001***	< 0.0001***	< 0.0001***	< 0.0001***	< 0.0001***	< 0.0001***

Highly significant differences were observed among treatments for all nutrients tested ($p < 0.0001$***), indicating strong treatment effects on nutrient uptake and accumulation. Categories marked with ***, **, and ° denote significance at $p < 0.001$, $p < 0.01$, and $0.1 < p < 1$ levels, respectively.

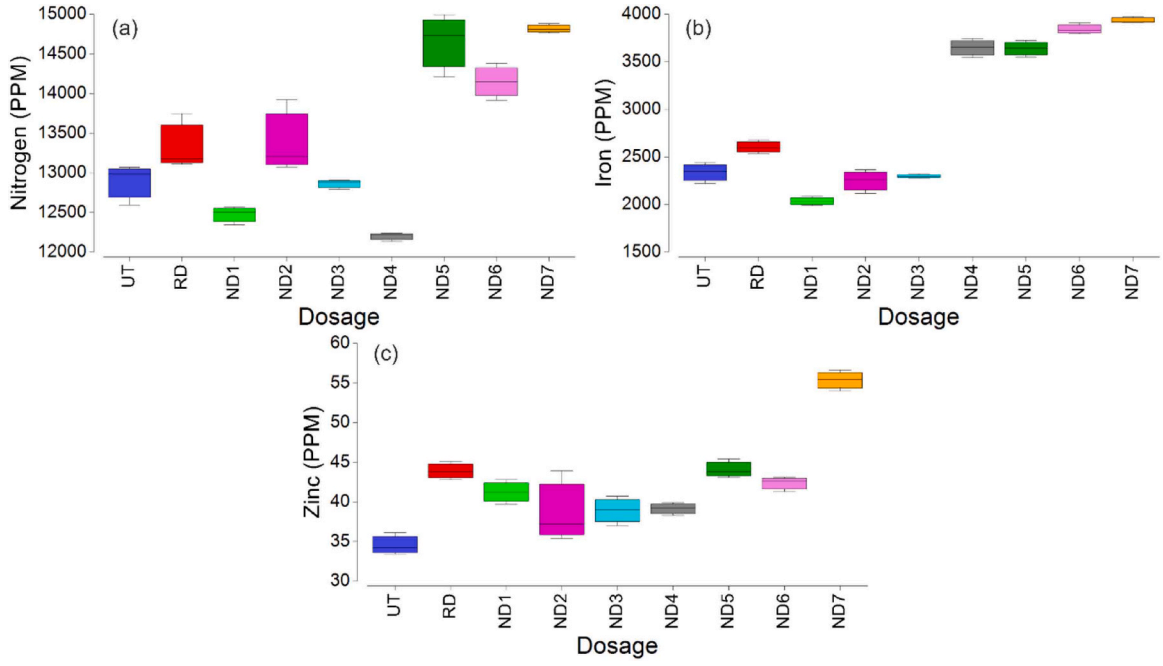

Fig. 7. (a) N, (b) Fe, and (c) Zn content in the shoots of the harvested Rosemary plants as a function of different dosages used to grow the Rosemary plants.

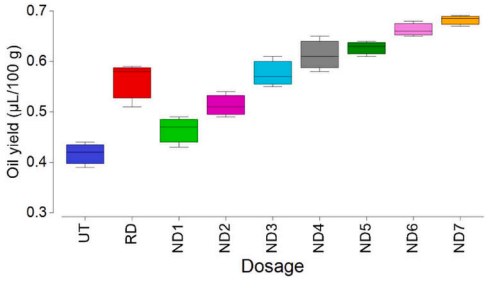

Fig. 8. Rosemary oil yield versus dosages used to grow the respective Rosemary plants.

consequences. The quality of Rosemary EO was assessed by analyzing the six prominent metabolites, alpha (α)-pinene, beta (β)-pinene, camphene, linalool, 1,8-cineole, and camphor, in each dosage case. Fig. 9 shows the metabolite contents as a function of different dosages used to grow the Rosemary plants. It may be noted that Rosemary EO may typically be constituted by 32 compounds, of which 1,8-cineole is the most abundant (Dhouibi et al., 2023; Laiq-ur-Rahman et al., 2007). It may also be noted that camphor is the second most abundant compound in local Rosemary oil (Laiq-ur-Rahman et al., 2007). The distinguishing characteristic of the premium Rosemary EO is its elevated concentration of 1,8-cineole and reduced levels of α-pinene and camphor (Dhouibi et al., 2023; Laiq-ur-Rahman et al., 2007). From Fig. 9, it was observed that camphor dominates in the UT case. On the other hand, the supply of RD of macro- and micro-nutrients improves the NUE, thereby enhancing the Rosemary plant's physiology (i.e., tissue development and metabolic activities), consequently increasing the 1,8-cineole content over camphor content in the oil, but with a compromise of increased α-pinene content. In correlation with the improved herbage (Figs. 5 and 6), NUE (Table 1 and Fig. 7), and Rosemary oil yield (Fig. 8), it can be observed from Fig. 9 that the 1,8-cineole content has increased along with the decrease in camphor content in ND3 to ND7 cases compared with RD. α-pinene content also decreased in ND3, ND4 and ND7 cases compared with RD. α-pinene content in the case of ND5 is similar to that of the RD case. The anomalous increase in the α-pinene content in ND5 and ND6 cases has to be further investigated. No prominent observations are made regarding the content of other metabolites, β-pinene, camphene, and linalool. The highest 1,8-cineole content of about 28 % (> 23 % corresponding to local RD) (Laiq-ur-Rahman et al., 2007) was measured

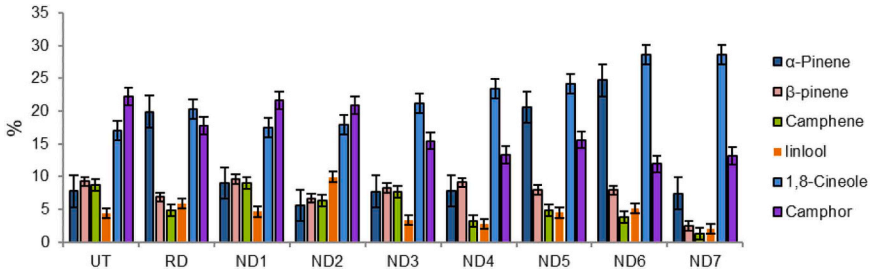

Fig. 9. Content of various metabolites by volume in the extracted Rosemary oils versus dosages used to grow the respective Rosemary plants. Only those > 2 % by volume are shown.

in the Rosemary oils corresponding to ND6 and ND7 cases. However, in the ND7 case, the α-pinene and camphor contents are lower than in all other dosage cases, implying that ND7 yields high-quality Rosemary EO. The ND7 case may have influenced terpene synthase activity or altered the allocation of metabolic precursors within the synthesis pathway, favouring specific monoterpene profiles. However, it is important to note that there is no mechanistic information in the literature regarding nutrient-mediated regulation of monoterpene biosynthesis in Rosemary, and the present explanation is based on plausible biochemical reasoning supported by studies in other plants, as explained in the next paragraph. The ND5 case also results in Rosemary EO with enhanced overall quality compared with the RD case.

Recently, it was shown that the foliar application of micro-nutrients positively affects 1,8-cineole content in Eucalyptus essential oil (Sakallı Ak, et al., 2022). However, such a study has to be conducted in the case of Rosemary. The hypothesis posits that all micronutrients, including Fe, Zn, Mn, Cu, and B, are directly or indirectly involved in several metabolic and gene regulation processes. In plants, 1,8-cineole biosynthesis is a composite process that begins with the synthesis of geranyl diphosphate through the mevalonate (MVA) pathway or methylerythritol phosphate pathway, then continues with the cyclization of geranyl diphosphate by 1,8-cineole synthase to generate the final product. In particular, 1,8-cineole synthase desires metal ions (such as Mn^{+2}) (Xu et al., 2023) or Zn^{+2} (EC no: 4.2.3.108; ENZYME - Enzyme nomenclature database of 1,8-cineole synthase. https://enzyme.expasy.org/EC/4.2.3.108) to synthesize 1,8-cineole from its precursor, geranyl diphosphate. It is also known that metal ions are essential cofactors in several metabolic pathways, including the MVA pathway (Frank and Groll, 2017; Kampranis et al., 2007). The Zn^{2+} ions, apart from their association with enzymes as cofactors, may regulate 1,8-cineole synthase gene expression by Zn finger transcription factors. Such Zn finger transcription factors with Zn^{2+} ions are shown to be responsible for terpenoid biosynthesis (Liu et al., 2023; Pauwels et al., 2008; Van Moerkercke et al., 2015). These works strongly suggest that increased Zn bioavailability in Rosemary may improve the 1,8-cineole content in the corresponding essential oil. In this work, as shown in Table 1, Cu bioavailability also increased in Rosemary. In this regard, it was shown that enhanced bioavailability of Cu can augment anthocyanin, chlorophyll, and carotenoid levels (Van Nguyen et al., 2022). The foliar application of nanosized Cu micro-nutrients improved critical secondary metabolites and the essential oil content in the case of Dragonhead plants (Nekoukhou et al., 2023). Additionally, foliar application of micro-nutrients can help in biofortification (Nekoukhou et al., 2022), which was also observed in this study (Table 1).

4. Conclusions

The conversion of conventional micron-sized nutrient particles into nanosized particles through optimized mechanical milling enhanced the surface accessibility and reactivity of essential plant nutrients. This nanosizing process increased the surface-associated nitrogen, iron, zinc, and copper, thereby improving their bioavailability to the plants without altering the original chemical composition of the fertilizers. The enhanced nutrient availability promoted more efficient nutrient uptake and assimilation by the rosemary plants, resulting in improved vegetative growth and a substantial increase in essential oil yield. This study demonstrates that nanoscale nutrient carriers enable more effective nutrient interaction with the root–soil interface, which in turn stimulates the biosynthetic pathways governing terpenoid formation. The observed increase in 1,8-cineole content and the associated modulation of α-pinene and camphor concentrations indicate that nanoscale nutrient delivery can influence the enzymatic balance within the secondary metabolite network of Rosemary. This finding validates the hypothesis that particle size–dependent nutrient bioavailability can regulate both quantitative and qualitative aspects of plant secondary metabolism. The study highlights a novel route for achieving enhanced essential oil productivity and compositional tailoring through precise control of nutrient formulation at the nanoscale. The implications of this work extend to the development of next-generation fertilizer systems that ensure high efficiency at reduced dosages, thereby promoting both agricultural productivity and environmental sustainability. Future efforts should be directed toward establishing direct molecular and histochemical evidence of nutrient internalization within plant tissues to elucidate the complete mechanistic pathway underlying these effects.

CRediT authorship contribution statement

Chalasani Danteswari: Writing – original draft, Investigation, Formal analysis, Data curation. **Pullabhotla V. S. R. N. Sarma:** Writing – original draft, Investigation, Formal analysis. **Harita Pant:** Writing – original draft, Investigation, Formal analysis. **Mahadevakumar Shivannegowda:** Writing – original draft, Investigation, Formal analysis. **Dharani Kumar Chennamsetty:** Writing – original draft, Investigation, Formal analysis. **Venkata Sreenivasulu Kummari:** Writing – original draft, Investigation, Formal analysis. **Vijaya Ranganath Chenna:** Investigation, Formal analysis. **Siddaiah Chandra Nayaka:** Investigation, Formal analysis. **Shaikshavali Petnikota:** Writing – review & editing, Resources, Investigation, Formal analysis. **Challapalli Subrahmanyam:** Writing – review & editing, Supervision, Resources, Methodology. **Venkata Satya Siva Srikanth Vadali:** Writing – review & editing, Methodology, Funding acquisition, Conceptualization. **Appa Rao Podile:** Writing – review & editing, Supervision, Methodology, Funding acquisition, Conceptualization.

Declaration of Competing Interest

The authors declare that they have no known competing financial interests or personal relationships that could have appeared to influence the work reported in this paper.

Acknowledgments

We thank DST-FIST for funding towards infrastructural facilities at the University of Hyderabad (UoH). ARP and VSSSV acknowledge the

financial support by the Department of Biotechnology (DBT), India, through Grant No. BT/PR36129/NNT/28/1708/2020. ARP and VSSSV also acknowledge "financial support to UoH-IoE by MHRD (F11/9/2019-U3(A))". The authors thank Dr. Vijaya Kumar Poondla, IIT Hyderabad, for recording XPS data. The authors sincerely thank the reviewers for their suggestions, which improved the quality of the work.

Appendix A. Supporting information

Supplementary data associated with this article can be found in the online version at doi:10.1016/j.indcrop.2025.122138.

Data availability

Data will be made available on request.

References

Afshar, M., Najafian, S., Radi, M., 2022. Seasonal variation on the major bioactive compounds: total phenolic and flavonoids contents, and antioxidant activity of rosemary from shiraz. Nat. Prod. Res. 36 (16), 4287–4292. https://doi.org/10.1080/14786419.2021.1978998.

Ahmed, K.B.M., Khan, M.M.A., Shabbir, A., Ahmad, B., Uddin, M., Azam, A., 2023a. Comparative effect of foliar application of silicon, titanium and zinc nanoparticles on the performance of vetiver- a medicinal and aromatic plant. Silicon 15 (1), 153–166. https://doi.org/10.1007/s12633-022-02007-9.

Ahmed, M.A., Shafiei-Masouleh, S.S., Mohsin, R.M., Salih, Z.K., 2023b. Foliar application of iron oxide nanoparticles promotes growth, mineral contents, and medicinal qualities of *solidago virgaurea* l. J. Soil Sci. Plant Nutr. 23 (2), 2610–2624. https://doi.org/10.1007/s42729-023-01218-2.

Ali, A., Oon, C.C., Chua, B.L., Figiel, A., Chong, C.H., Wojdylo, A., Turkiewicz, I.P., Szumny, A., Łyczko, J., 2020. Volatile and polyphenol composition, anti-oxidant, anti-diabetic and anti-aging properties, and drying kinetics as affected by convective and hybrid vacuum microwave drying of *rosmarinus officinalis* L. Ind. Crops Prod. 151, 112463. https://doi.org/10.1016/j.indcrop.2020.112463.

Ayoob, B., Singh, A., Gangoo, S.A., Malik, A.R., Raj, A., Akhter, A., Bilal, T., 2023. Effect of plant spacing and nitrogen levels on growth, yield and essential oil content of rosemary (*salvia rosmarinus* Spenn) under marginal land conditions. J. Essent. Oil Bear. Plants 2023 (26), 21–23. https://doi.org/10.1080/0972060X.2023.2171813.

Baer, D.R., Engelhard, M.H., 2010. XPS analysis of nanostructured materials and biological surfaces. J. Electron Spectros. Relat. Phenom. 178-179, 415–432. https://doi.org/10.1016/j.elspec.2009.09.003.

Baudot, C., Tan, C.M., Kong, J.C., 2010. FTIR spectroscopy as a tool for nano-material characterization. Infrared Phys. Technol. 53, 434–438. https://doi.org/10.1016/j.infrared.2010.09.002.

Bekah, D., Boyjoo, Y., Panpadoo, R.M., White, J.C., Bhaw-Luximon, A., 2025. Nanostimulants and nanofertilizers for precision agriculture: transforming food production in the 21st century. Environ. Sci. Nano 12, 1740–1766. https://doi.org/10.1039/D5EN00055F.

Bellamy, L.J., Gerrard, W., Lappert, M.F., Williams, R.L., 1958. 481. Infrared spectra of boron compounds. J. Chem. Soc. 2412–2415. https://doi.org/10.1039/JR9580002412.

Britto, D.T., Kronzucker, H.J., 2002. nh_4^+toxicity in higher plants: a critical review. J. Plant Physiol. 159, 567–584. https://doi.org/10.1078/0176-1617-0774.

Buciuman, F., Patcas, F., Craciun, R., Zahn, D.R.T., 1999. Vibrational spectroscopy of bulk and supported manganese oxides. Phys. Chem. Chem. Phys. 1, 185–190. https://doi.org/10.1039/A807821A.

Cao, X., Yue, L., Wang, C., Luo, X., Zhang, C., Zhao, X., Wu, F., White, J.C., Wang, Z., Xing, B., 2022. Foliar application with iron oxide nanomaterials stimulate nitrogen fixation, yield, and nutritional quality of soybean. ACS Nano 16 (1), 1170–1181 https://pubs.acs.org/doi/10.1021/acsnano.1c08977.

Chahine, A., Et-tabirou, M., Elbenaissi, M., Haddad, M., Pascal, J.L., 2004. Effect of CuO on the structure and properties of $(50-x/2)Na_2O$ xCuO $(50-x/2)P_2O_5$ glasses. Mater. Chem. Phys. 84, 341–347. https://doi.org/10.1016/j.matchemphys.2003.11.009.

Chen, L., Wang, M., Shi, Y., Ma, P., Xiao, Y., Yu, H., Ding, J., 2023. Soil phosphorus form affects the advantages that arbuscular mycorrhizal fungi confer on the invasive plant species, solidago canadensis, over its congener. Front. Microbiol 14, 1160631. https://doi.org/10.3389/fmicb.2023.1160631.

Dhouibi, I., Flamini, G., Bouaziz, M., 2023. Comparative study on the essential oils extracted from Tunisian rosemary and myrtle: chemical profiles, quality, and antimicrobial activities. ACS Omega 8, 6431–6438. https://doi.org/10.1021/acsomega.2c06713.

Ding, Y., Zhao, W., Zhu, G., Wang, Q., Zhang, P., Rui, Y., 2023. Recent trends in foliar nanofertilizers: a review. Nanomaterials 13, 2906. https://doi.org/10.3390/nano13212906.

Elmer, W.H., Zuverza-Mena, N., Triplett, L.R., Roberts, E.L., Silady, R.A., White, J.C., 2021. Foliar application of copper oxide nanoparticles suppresses fusarium wilt development on chrysanthemum. Environ. Sci. Technol. 55 (15), 10805–10810. https://doi.org/10.1021/acs.est.1c02323.

Esteban, R., Ariz, I., Cruz, C., Moran, J.F., 2016. Review: mechanisms of ammonium toxicity and the quest for tolerance. Plant Sci. 248, 92–101. https://doi.org/10.1016/j.plantsci.2016.04.008.

Fairley, N., Fernandez, V., Richard-Plouet, M., Guillot-Deudon, C., Walton, J., Smith, E., Flahaut, D., Greiner, M., Biesinger, M., Tougaard, S., Morgan, D., Baltrusaitis, J., 2021. Systematic and collaborative approach to problem solving using X-ray photoelectron spectroscopy. Appl. Surf. Sci. Adv. 5, 100112. https://doi.org/10.1016/j.apsadv.2021.100112.

Frank, A., Groll, M., 2017. The methylerythritol phosphate pathway to isoprenoids. Chem. Rev. 117 (8), 5675–5703. https://doi.org/10.1021/acs.chemrev.6b00537.

Ghodrati-Tazangi, M.J., Samani, R.B., Tavallali, V., Alizadeh, A., Honarvar, M., 2023. Responses of *hyssopus officinalis* to bicarbonate stress and foliar application of Green synthesized zinc nano-complex formed on *medicago sativa* extract. Sci. Hortic. 319, 112197. https://doi.org/10.1016/j.scienta.2023.112197.

Grusak, M.A., DellaPenna, D., 1999. Improving the nutrient composition of plants to enhance human nutrition and health. Annu. Rev. Plant Physiol. 50, 133–161. https://doi.org/10.1146/annurev.arplant.50.1.133.

Guo, H., White, J.C., Wang, Z., Xing, B., 2018. Nano-enabled fertilizers to control the release and use efficiency of nutrients. Curr. Opin. Environ. Sci. Hl. 6, 77–83. https://doi.org/10.1016/j.coesh.2018.07.009.

Hammer, M., Junghanns, W., 2020. *rosmarinus officinalis* L.: rosemary. In: Novak, J., Blüthner, W.D. (Eds.), Medicinal, Aromatic and Stimulant Plants. Handbook of Plant Breeding, 12. Springer, Cham. https://doi.org/10.1007/978-3-030-38792-1_15.

Hao, B., Ma, J., Jiang, L., Wang, X., Bai, Y., Zhou, C., Ren, S., Li, C., Wang, Z., 2021. Effects of foliar application of micronutrients on concentration and bioavailability of zinc and iron in wheat landraces and cultivars. Sci. Rep. 11, 22782. https://doi.org/10.1038/s41598-021-02088-3.

Hassanpouraghdam, M.B., Mehrabani, L.V., Tzortzakis, N., 2020. Foliar application of nano-zinc and iron affects physiological attributes of *rosmarinus officinalis* and quietens NaCl salinity depression. J. Soil Sci. Plant Nutr. 20 (2), 335–345. https://doi.org/10.1007/s42729-019-00111-1.

Heinrich, M., Kufer, J., Leonti, M., Pardo-de-Santayana, M., 2006. Ethnobotany and ethnopharmacology–interdisciplinary links with the historical sciences. J. Ethnopharmacol. 107 (2), 157–160. https://doi.org/10.1016/j.jep.2006.05.035.

Jackson, L.E., Burger, M., Cavagnaro, T.R., 2008. Roots, nitrogen transformations, and ecosystem services. Annu. Rev. Plant Biol. 59, 341–363. https://doi.org/10.1146/annurev.arplant.59.032607.092932.

Jakhar, A.M., Aziz, I., Kaleri, A.R., Hasnain, M., Haider, G., Ma, J., Abideen, Z., 2022. Nano-fertilizers: a sustainable technology for improving crop nutrition and food security. NanoImpact 27, 100411. https://doi.org/10.1016/J.IMPACT.2022.100411.

Jayawardena, H.S.N., Liyanage, S.H., Rathnayake, K., Patel, U., Yan, M., 2021. Analytical methods for characterization of nanomaterial surfaces. Anal. Chem. 93 (4), 1889–1911. https://doi.org/10.1021/acs.analchem.0c05208.

Kamble, S., Agrawal, S., Cherumukkil, S., Sharma, V., Jasra, R.V., Munshi, P., 2022. Revisiting zeta potential, the key feature of interfacial phenomena, with applications and recent advancements. ChemistrySelect 7, e202103084. https://doi.org/10.1002/slct.202103084.

Kampranis, S.C., Ioannidis, D., Purvis, A., Mahrez, W., Ninga, E., Katerelos, N.A., Anssour, S., Dunwell, J.M., Degenhardt, J., Makris, A.M., Goodenough, P.W., Johnson, C.B., 2007. Rational conversion of substrate and product specificity in a *salvia* monoterpene synthase: structural insights into the evolution of terpene synthase function. Plant Cell 19, 1994–2005. https://doi.org/10.1105/tpc.106.047779.

Kayani, Z.N., Umer, M., Riaz, S., Naseem, S., 2015. Characterization of copper oxide nanoparticles fabricated by the sol–gel method. J. Electron. Mater. 44, 3704–3709. https://doi.org/10.1007/s11664-015-3867-5.

Laiq-ur-Rahman, L.U.R., Kukerja, A.K., Singh, S.K., Anand Singh, A.S., Anju Yadav, A.Y., Khanuja, S.P.S., 2007. Qualitative analysis of essential oil of *rosmarinus officinalis* L. Cultivated in uttaranchal hills. India J. Spices Arom. Crops 16, 55–57. ⟨https://updatepublishing.com/journal/index.php/josac/article/view/4870⟩. Accessed: 13 April 2025.

Li, J., Wang, Z., Zhang, Y., Cao, X., Lian, F., Gu, S., 2023. Novel selenium-doped carbon quantum dots derived from algae effectively enhanced the delivery and accumulation of selenium in tomato plants (*lycopersicum esculentum*) via foliar application. Environ. Sci. Nano 10 (3), 866–878. https://doi.org/10.1039/D2EN00918H.

Liu, Y., von Wirén, N., 2017. Ammonium as a signal for physiological and morphological responses in plants. J. Exp. Bot. 68 (1), 2581–2592. https://doi.org/10.1093/jxb/erx086.

Lowry, G.V., Giraldo, J.P., Steinmetz, N.F., Avellan, A., Demirer, G.S., Ristroph, K.D., Wang, G.J., Hendren, C.O., Alabi, C.A., Caparco, A., da Silva, W., González-Gamboa, I., Grieger, K.D., Jeon, S.-J., Khodakovskaya, M.V., Kohay, H., Kumar, V., Muthuramalingam, R., Poffenbarger, H., Santra, S., Tilton, R.D., White, J.C., 2024. Towards realizing nano-enabled precision delivery in plants. Nat. Nanotechnol. 19, 1255–1269. https://doi.org/10.1038/s41565-024-01667-5.

Magdalena, A.G., Silva, I.M.B., Marques, R.F.C., Pipi, A.R.F., Lisboa-Filho, P.N., Jafelicci Jr, M., 2018. EDTA-functionalized Fe_3O_4 nanoparticles. J. Phys. Chem. Solids 113, 5–10. https://doi.org/10.1016/j.jpcs.2017.10.002.

Magdas, D.A., Cozar, O., Chis, V., Ardelean, I., Vedeanu, N., 2008. The structural dual role of Fe_2O_3 in some lead-phosphate glasses. Vib. Spectrosc. 48, 251–254. https://doi.org/10.1016/j.vibspec.2008.02.016.

Mehrabani, L.V., Hassanpouraghdam, M.B., Shamsi-Khotab, T., 2018. The effects of common and nano-zinc foliar application on the alleviation of salinity stress in *rosmarinus officinalis* L. Acta Sci. Pol. Hortorum Cultus 17 (6), 65–73. https://doi.org/10.24326/asphc.2018.6.7.

Mim, J.J., Maksudur Rahman, S.M., Khan, F., Paul, D., Sikder, S., Das, H.P., Khan, S., Orny, N.T., Shuvo, M.R.H., Hossain, N., 2025. Towards smart agriculture through nano-fertilizer-A review. Mater. Today Sustain. 30, 101100. https://doi.org/10.1016/j.mtsust.2025.101100.

Mokhele, B., Zhan, X., Yang, G., Zhang, X., 2012. Review: Nitrogen assimilation in crop plants and its affecting factors. Can. J. Plant Sci. 92 (3), 399–405. https://doi.org/10.4141/cjps2011-135.

Mosa, W.F.A., El-Shehawi, A.M., Mackled, M.I., Salem, M.Z.M., Ghareeb, R.Y., Hafez, E. E., Behiry, S.I., Abdelsalam, N.R., 2021. Productivity performance of peach trees, insecticidal and antibacterial bioactivities of leaf extracts as affected by nanofertilizers foliar application. Sci. Rep. 11 (1), 10205. https://doi.org/10.1038/s41598-021-89885-y.

Moulder, J.F., Stickle, W.F., Sobol, P.E., Bomben, K.D., 1992. Handbook of X-Ray photoelectron spectroscopy: a reference book of standard spectra for identification and interpretation of XPS data. Perkin-Elmer Corporation (Physical Electronics Division), Eden Prairie, Minnesota.

Mwithiga, G., Maina, S., Gitari, J., Muturi, P., 2022. Rosemary (*rosmarinus officinalis* L.) growth rate, oil yield and oil quality under differing soil amendments. Heliyon 8 (4), e09277. https://doi.org/10.1016/j.heliyon.2022.e09277.

Namduri, H., Nasrazadani, S., 2008. Quantitative analysis of iron oxides using Fourier transform infrared spectrophotometry. Corros. Sci. 50 (9), 2493–2497. https://doi.org/10.1016/j.corsci.2008.06.034.

Nazri, G.A., Julien, C., 1992. Far-infrared and Raman studies of orthorhombic MoO_3 single crystal. Solid State Ion. 53-56 (Part 1), 376–382. https://doi.org/10.1016/0167-2738(92)90403-C.

Nekoukhou, M., Fallah, S., Abbasi-Surki, A., Pokhrel, L.R., Rostamnejadi, A., 2022. Improved efficacy of foliar application of zinc oxide nanoparticles on zinc biofortification, primary productivity and secondary metabolite production in dragonhead. J. Clean. Prod. 379, 134803. https://doi.org/10.1016/J.JCLEPRO.2022.134803.

Nekoukhou, M., Fallah, S., Pokhrel, L.R., Abbasi-Surki, A., Rostamnejadi, A., 2023. Foliar enrichment of copper oxide nanoparticles promotes biomass, photosynthetic pigments, and commercially valuable secondary metabolites and essential oils in dragonhead (*dracocephalum moldavica* L.) under semi-arid conditions. Sci. Total Environ. 863, 160920. https://doi.org/10.1016/j.scitotenv.2022.160920.

Pauwels, L., Morreel, K., De Witte, E., Lammertyn, F., Van Montagu, M., Boerjan, W., Inzé, D., Goossens, A., 2008. Mapping methyl jasmonate-mediated transcriptional reprogramming of metabolism and cell cycle progression in cultured arabidopsis cells. Proc. Natl. Acad. Sci. 105 (4), 1380–1385. https://doi.org/10.1073/pnas.0711203105.

Pohshna, C., Mailapalli, D.R., Laha, T., 2020. Synthesis of nanofertilizers by planetary ball milling, 40. In: Lichtfouse, E. (Ed.), Sustainable Agriculture Reviews, 40. Springer, Cham, Switzerland, pp. 75–112, 40.

Pudhuvai, B., Koul, B., Das, R., Shah, M.P., 2025. Nano-fertilizers (NFs) for resurgence in nutrient use efficiency (NUE): a sustainable agricultural strategy. Curr. Pollut. Rep. 11, 1. https://doi.org/10.1007/s40726-024-00331-9.

Puttanna, K., Prakasa Rao, E.V.S., Singh, R., Ramesh, S., 2010. Influence of nitrogen and potassium fertilization on yield and quality of rosemary in relation to harvest number. Commun. Soil Sci. Plant Anal. 41, 190–198. https://doi.org/10.1080/00103620903429984.

Rathore, S., Mukhia, S., Kapoor, S., Bhatt, V., Kumar, R., Kumar, R., 2022. Seasonal variability in essential oil composition and biological activity of *rosmarinus officinalis* L. Accessions in the Western himalaya. Sci. Rep. 12, 3305. https://doi.org/10.1038/s41598-022-07298-x.

Reshma, Z., Meenal, K., 2022. Foliar application of biosynthesised zinc nanoparticles as a strategy for ferti-fortification by improving yield, zinc content and zinc use efficiency in amaranth. Heliyon 8 (10), e10912. https://doi.org/10.1016/j.heliyon.2022.e10912.

Ribeiro-Santos, R., Carvalho-Costa, D., Cavaleiro, C., Costa, H.S., Albuquerque, T.G., Castilho, M.C., Ramos, F., Melo, N.R., Sanches-Silva, A., 2015. A novel insight on an ancient aromatic plant: the rosemary (*rosmarinus officinalis* L.). Trends Food Sci. Technol. 45 (2), 355–368. https://doi.org/10.1016/J.TIFS.2015.07.015.

Rostami, M., Davari, M.R., Movahedi, Z., Siahpoosh, S., 2021. Changes in morpho-physiological characteristics of peppermint by foliar application of biofertilizer and nanofertilizers. Agric. Environ. Soc. 1 (1), 57–62. https://doi.org/10.22034/AES.2022.322455.1012.

Sahrawat, K.L., Kumar, G.R., Murthy, K.V.S., 2002. Sulfuric acid–selenium digestion for multi-element analysis in a single plant digest. Commun. Soil Sci. Plant Anal. 33 (19-20), 3757–3765. https://doi.org/10.1081/CSS-120015920.

Sakallı Ak, E., Teralı, K., Karadağ, A.E., Biltekin, S.N., Koşar, M., Demirci, B., Hüsnü Can Başer, K., Demirci, F., 2022. In vitro and in silico evaluation of ACE2 and LOX inhibitory activity of eucalyptus essential oils, 1,8-Cineole, and citronellal. Nat. Prod. Commun. 17, 1. https://doi.org/10.1177/1934578X221109409.

Salim, M.A., Khattak, G.D., Hussain, M.S., 1995. X-ray photoelectron spectroscopy, Fourier transform infrared spectroscopy and electrical conductivity studies of copper phosphate glasses. J. Non Cryst. Solids 185 (1-2), 101–108. https://doi.org/10.1016/0022-3093(94)00683-0.

Serrano-Lotina, A., Portela, R., Baeza, P., Alcolea-Rodriguez, V., Villarroel, M., Ávila, P., 2023. Zeta potential as a tool for functional materials development. Catal. Today 423, 113862. https://doi.org/10.1016/j.cattod.2022.08.004.

Shan, L., Oduor, A.M.O., Huang, W., Liu, Y., 2022. Nutrient enrichment promotes invasion success of alien plants via increased growth and suppression of chemical defenses. Ecol. Appl. 34 (1), e2791. https://doi.org/10.1002/eap.2791.

Sharma, S.K., Sharma, P.K., Mandeewal, R.L., Sharma, V., Chaudhary, R., Pandey, R., Gupta, S., 2022. Effect of foliar application of nano-urea under different nitrogen levels on growth and nutrient content of pearl millet (*pennisetum glaucum* L.). Int. J. Plant Soil Sci. 30 (20), 149–155. https://doi.org/10.9734/ijpss/2022/v34i2031138.

Shih, P.Y., Yung, S.W., Chin, T.S., 1999. FTIR and XPS studies of P_2O_5–Na_2O–CuO glasses. J. Non Cryst. Solids 244 (2-3), 211–222. https://doi.org/10.1016/S0022-3093(99)00011-3.

Shilpha, J., Song, J., Jeong, B.R., 2023. Ammonium phytotoxicity and tolerance: an insight into ammonium nutrition to improve crop productivity. Agronomy 13 (6), 1487. https://doi.org/10.3390/agronomy13061487.

Suryanarayana, C., 2001. Mechanical alloying and milling. Prog. Mater. Sci. 46 (1-2), 1–184. https://doi.org/10.1016/S0079-6425(99)00010-9.

Tawfeeq, A., Culham, A., Davis, F., Reeves, M., 2016. Does fertilizer type and method of application cause significant differences in essential oil yield and composition in rosemary (*rosmarinus officinalis* L.)? Ind. Crop. Prod. 88, 17–22. https://doi.org/10.1016/j.indcrop.2016.03.026.

Timón, V., Maté, B., Herrero, V.J., Tanarro, I., 2021. Infrared spectra of amorphous and crystalline urea ices. Phys. Chem. Chem. Phys. 23, 22344–22351. https://doi.org/10.1039/D1CP03503G.

Ulbricht, C., Abrams, T.R., Brigham, A., Ceurvels, J., Clubb, J., Curtiss, W., Kirkwood, C. D., Giese, N., Hoehn, K., Iovin, R., Isaac, R., Rusie, E., Serrano, J.M.G., Varghese, M., Weissner, W., Windsor, R.C., 2010. An evidence-based systematic review of rosemary (*rosmarinus officinalis*) by the natural standard research collaboration. J. Diet. Suppl. 7 (4), 351–413. https://doi.org/10.3109/19390211.2010.525049.

Van Moerkercke, A., Steensma, P., Schweizer, F., Pollier, J., Gariboldi, I., Payne, R., Vanden Bossche, R., Miettinen, K., Espoz, J., Purnama, P.C., Kellner, F., Seppänen-Laakso, T., O'Connor, S.E., Rischer, H., Memelink, J.A., 2015. The bHLH transcription factor BIS1 controls the iridoid branch of the monoterpenoid indole alkaloid pathway in catharanthus roseus. Proc. Natl. Acad. Sci. 112 (26), 8130–8135. https://doi.org/10.1073/pnas.1504951112.

Van Nguyen, D., Nguyen, H.M., Le, N.T., Nguyen, K.H., Nguyen, H.T., Le, H.M., Nguyen, A.T., Dinh, N.T.T., Hoang, S.A., Van Ha, C., 2022. Copper nanoparticle application enhances plant growth and grain yield in maize under drought stress conditions. J. Plant Growth Regul. 41, 364–375. https://doi.org/10.1007/s00344-021-10301-w.

Weinmann, M., Bradáčová, K., Nikolic, M., 2023. Chapter 10 - relationship between mineral nutrition, plant diseases, and pests. In: Rengel, Z., Cakmak, I., White, P.J. (Eds.), Marschner's Mineral Nutrition of Plants, Fourth Edition. Academic Press, pp. 445–476. https://doi.org/10.1016/B978-0-12-819773-8.00009-5.

Wheal, M.S., Fowles, T.O., Palmer, L.T., 2011. A cost-effective acid digestion method using closed polypropylene tubes for inductively coupled plasma optical emission spectrometry (ICP-OES) analysis of plant essential elements. Anal. Methods 3, 2854–2863. https://doi.org/10.1039/c1ay05430a.

Wu, H.B., Chan, M.N., Chan, C.K., 2007. FTIR characterization of polymorphic transformation of ammonium nitrate. Aerosol Sci. Technol. 41, 581–588. https://doi.org/10.1080/02786820701272038.

Xiong, G., Pal, U., Serrano, J.G., Ucer, K.B., Williams, R.T., 2006. Photoluminesence and FTIR study of ZnO nanoparticles: The impurity and defect perspective. Phys. Status Solidi C 3 (10), 3577–3581. https://doi.org/10.1002/pssc.200672164.

Xu, G., Zheng, Q., Wei, P., Zhang, J., Liu, P., Zhang, H., Zhai, N., Li, X., Xu, X., Chen, Q., Cao, P., Zhao, J., Zhou, H., 2023. Metabolic engineering of a 1,8-cineole synthase enhances aphid repellence and increases trichome density in transgenic tobacco (*nicotiana tabacum* L.). Pest Manag. Sci. 79 (9), 3342–3353. https://doi.org/10.1002/ps.7520.

Xu, X., Liang, A., Li, H., Shang, H., Qian, K., Jia, W., White, J.C., Ma, C., Xing, B., 2023. Foliar applied ZnO quantum dots boost pumpkin (*cucurbita moschata duch.*) growth and positively alter endophytic and rhizosphere microbial communities. ACS Sustain. Chem. Eng. 11 (23), 8503–8516. https://doi.org/10.1021/acssuschemeng.3c00954.

Yang, R., Wang, Z., Dai, L., Chen, L., 2005. Synthesis and characterization of single-crystalline nanorods of α-MnO_2 and γ-MnOOH. Mater. Chem. Phys. 93 (1), 149–153. https://doi.org/10.1016/j.matchemphys.2005.03.006.